


Impact of Isomeric Structures on Transistor Performances in Naphthodithiophene Semiconducting Polymers

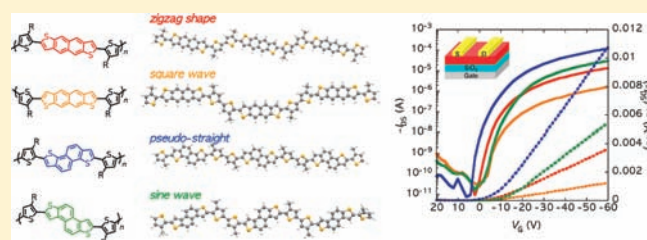
Itaru Osaka,^{*,†} Toru Abe,[†] Shoji Shinamura,[†] and Kazuo Takimiya^{*,†,‡}

[†]Department of Chemistry, Graduate School of Engineering, Hiroshima University, 1-4-1 Kagamiyama, Higashi-Hiroshima, Hiroshima 739-8527, Japan

[‡]Institute for Advanced Materials Research, Hiroshima University, Higashi-Hiroshima 739-8530, Japan

 Supporting Information

ABSTRACT: Four isomeric naphthodithiophenes (NDTs) with linear and angular shapes were introduced into the polythiophene semiconductor backbones, and their field-effect transistor performances were characterized. The polymers bearing naphtho[1,2-*b*:5,6-*b'*]dithiophene (NDT3), an angular-shaped NDT, exhibited the highest mobilities of $\sim 0.8 \text{ cm}^2 \text{ V}^{-1} \text{ s}^{-1}$ among the four NDT-based polymers, which is among the highest reported so far for semiconducting polymers. Interestingly, the trend of the mobility in the NDT-based polymers was contrary to our expectations; the polymers with angular NDTs showed higher mobilities than those with linear NDTs despite the fact that naphtho[2,3-*b*:6,7-*b'*]dithiophene (NDT1), a linear-shaped NDT, has shown the highest mobility in small-molecule systems. X-ray diffraction studies revealed that angular-NDT-based polymers gave the highly ordered structures with a very close π -stacking distance of 3.6 Å, whereas linear-NDT-based polymers had a very weak or no π -stacking order, which is quite consistent with the trend of the mobility. The nature of such ordering structures can be well understood by considering their molecular shapes. In fact, a linear NDT (NDT1) provides angular backbones and an angular NDT (NDT3) provides a pseudostraight backbone, the latter of which can pack into the highly ordered structure and thus facilitate the charge carrier transport. In addition to the ordering structure, the electronic structures seem to correlate with the carrier transport property. MO calculations, supported by the measurement of ionization potentials, suggested that, while the HOMOs are relatively localized within the NDT cores in the linear-NDT-based polymers, those are apparently delocalized along the backbone in the angular-NDT-based polymers. The latter should promote the efficient HOMO overlaps between the polymer backbones that are the main paths of the charge carrier transport, which also agrees with the trend of the mobility. With these results, we conclude that angular NDTs, in particular NDT3, are promising cores for high-performance semiconducting polymers. We thus propose that both the molecular shapes and the electronic structures are important factors to be considered when designing high performance semiconducting polymers.



INTRODUCTION

Organic field-effect transistors (OFETs) have been attracting considerable attention over the past decades because of the potential application to large area flexible displays or ubiquitous cheap electronics, so as to differentiate from the conventional silicon technologies.^{1–4} Of particular interest today is the use of soluble semiconductors that can be formulated as inks and patterned by printing technologies, offering great advantages to manufacture.^{5–7} With the excellent solution processability, film uniformity, and thermal stability, π -conjugated semiconducting polymers are a promising choice to commercialize these devices.^{8–11} The most important parameter for OFETs is the charge carrier mobility, how fast the injected carriers travel through the π -orbital overlap of the molecules within the transistor channel. It is therefore crucial to control the π – π interaction, typically described as π -stacking, of the polymer backbones to achieve higher mobilities in semiconducting polymer-based OFETs.¹²

Regioregular poly(3-hexylthiophene) (rrP3HT, Figure 1),^{13–15} a most widely studied semiconducting polymer to date, has provided essential guidance for designing this class of polymers; the head-to-tail regio-controlled polymerization of the monomer unit achieves a coplanar backbone, forming a highly crystalline microstructures (lamellar and π -stacking structures). The distance of π -stacking (d_π) is as close as ca. 3.8 Å, which plays an important role in its high charge carrier mobilities typically ranging from 0.01 to 0.1 $\text{cm}^2 \text{ V}^{-1} \text{ s}^{-1}$.¹⁶ On the other hand, regiosymmetric polythiophenes,¹⁷ the repeat units of which consist of unsubstituted thiophene(s) sandwiched by two alkylthiophenes in “head-to-head” symmetric fashion such as poly(3,3'-didodecylquaterthiophene) (PQT-12, Figure 1),¹⁸ are also important polymers in this class. The advantage of the motif is that a free space generated by the

Received: February 20, 2011

Published: April 08, 2011

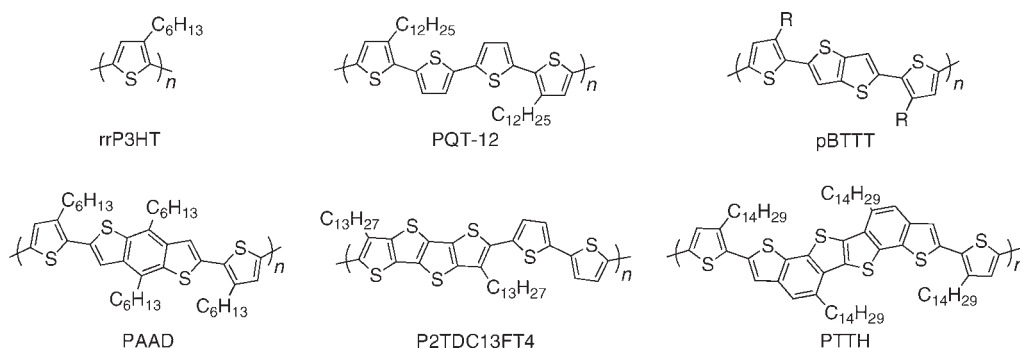
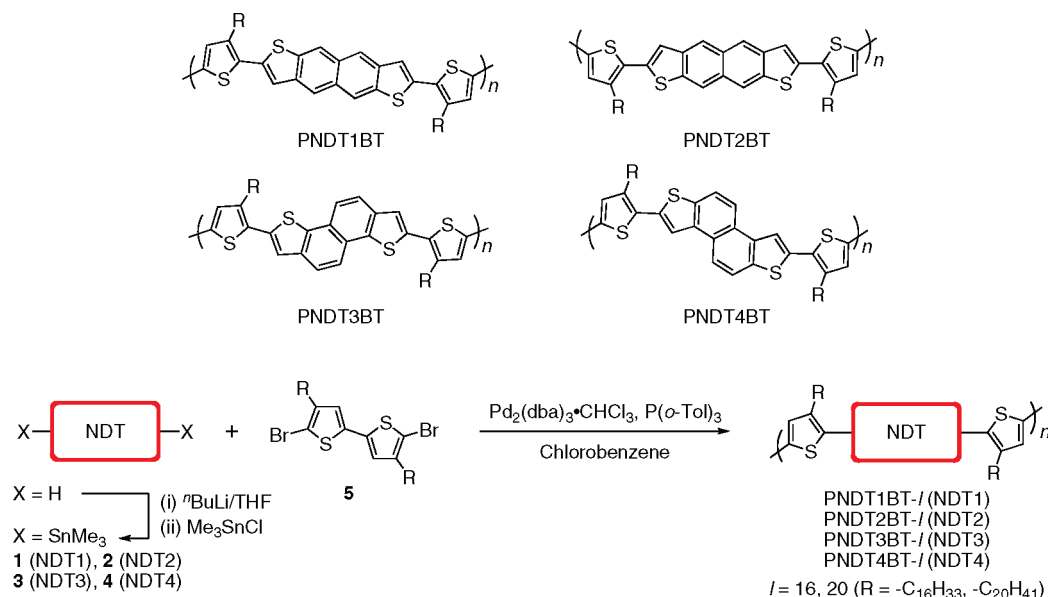


Figure 1. Chemical structures of polythiophenes and thiophene-based semiconducting polymers with heteroarenes.

Scheme 1. Chemical Structures of and Synthetic Route to the Naphthodithiophene-Based Semiconducting Polymers



unsubstituted thiophenes is likely to allow side chain interdigitation between adjacent polymer chains, which would give rise to a more highly ordered microstructure, in turn yielding higher mobilities relative to rrP3HT.¹⁹ Furthermore, incorporation of thiophene-based fused aromatic rings (heteroarenes) into the regiosymmetric polythiophene motif can give even higher mobilities due to the enhanced coplanarity, and thus π -stacking of the backbone as represented by poly(2,5-bis(3-alkylthiophen-2-yl)thieno[3,2-*b*]thiophene)s (pBTTTs, Figure 1);^{20,21} pBTTTs have been reported to possess strong π -stacking with a narrow d_{π} of 3.7 Å²² and to demonstrate the mobility of $\sim 0.5 \text{ cm}^2 \text{ V}^{-1} \text{ s}^{-1}$, and later the mobility has reached $1.0 \text{ cm}^2 \text{ V}^{-1} \text{ s}^{-1}$ by device optimizations.^{23,24} Further π -extended heteroarenes are then introduced into the polythiophene backbone,^{25–33} as well as the construction of donor–acceptor backbone,^{34–41} expecting the improvement of charge carrier mobilities. However, an extension of the fused ring system is not always effective in the mobility improvement. For instance, polymers bearing benzodithiophene, a three-ring-fused heteroarene (PAAD),²⁵ and tetrathienoacene, a four-ring-fused heteroarene (P2TDC13FT4),²⁹ show mobilities of $0.3 \text{ cm}^2 \text{ V}^{-1} \text{ s}^{-1}$ at most, and the polymer with tetrahexaene, a six-ring-fused heteroarene, shows limited mobilities of $\sim 10^{-3} \text{ cm}^2 \text{ V}^{-1} \text{ s}^{-1}$.³³ In addition, the backbone geometry influences

the transistor performances of semiconducting polymers as studied by Rieger et al. using various benzodithiophene isomers as the heteroarene core.⁴² Hence, careful design of heteroarenes is necessary for the development of high performance semiconducting polymers.

Recently, we have reported on a novel semiconducting polymer system, poly(2,7-bis(3-alkylthiophen-2-yl)naphtho[1,2-*b*:5,6-*b'*]dithiophene)s (PNDD3BTs, Scheme 1).⁴³ With highly π -extended naphtho[1,2-*b*:5,6-*b'*]dithiophene (NDT3),⁴⁴ a four-ring-fused heteroarene consisting of two thiophenes and two benzenes, these regiosymmetric polymers formed highly crystalline and close π -stacking (3.6 Å) structures and exhibited charge carrier mobilities as high as $0.54 \text{ cm}^2 \text{ V}^{-1} \text{ s}^{-1}$. We also found that while NDT3 gave lower mobilities by an order of magnitude than those for [1]benzothieno[3,2-*b*][1]benzothiophene (BTBT),^{45–47} an isomeric structure of NDT3, in small-molecule systems, NDT3 gave far superior OFET properties as compared to BTBT in the polymer system; actually, BTBT-based polymer did not work as the OFET material. This result is most likely understood by the difference of steric impact evident from the absorption spectra and also shows the importance of choice of heteroarenes to create high performance semiconducting polymers.

Recently, we have successfully developed facile and selective syntheses of three other naphthodithiophene (NDT) isomers,

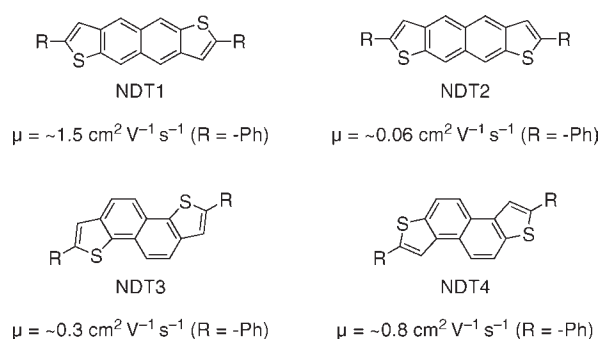


Figure 2. Four isomeric naphthodithiophenes: naphtho[2,3-*b*:6,7-*b'*]dithiophene (NDT1), naphtho[2,3-*b*:7,6-*b'*]dithiophene (NDT2), naphtho[1,2-*b*:5,6-*b'*]dithiophene (NDT3), and naphtho[2,1-*b*:6,5-*b'*]dithiophene (NDT4) ($R = -H, -C_8H_{17}, -Ph$).

naphtho[2,3-*b*:6,7-*b'*]dithiophene (NDT1), naphtho[2,3-*b*:7,6-*b'*]dithiophene (NDT2), and naphtho[2,1-*b*:6,5-*b'*]dithiophene (NDT4), as shown in Figure 2.⁴⁸ Interestingly, linear-shaped NDTs (NDT1 and NDT2) and angular-shaped NDTs (NDT3 and NDT4) provided quite different electronic structures and crystal structures, and thus OFET performances; NDT1 with two phenyl groups exhibited the highest mobility of $\sim 1.5 \text{ cm}^2 \text{ V}^{-1} \text{ s}^{-1}$ among the four NDTs. In addition, although NDT1 and NDT2 have similar molecular shapes and electronic structures, the charge carrier transport properties were quite distinct. These interesting results prompt us to examine the potentials of NDT isomers in the polymer systems and to explore new semiconducting polymers with even higher performances. We herein report the synthesis of the series of NDT-based semiconducting polymers with four different isomeric NDTs and discuss the impact of isomeric structures on the electronic structures, ordering structures in the thin film, and the OFET properties.

RESULTS AND DISCUSSION

Synthesis and Chemical/Thermal Properties. Scheme 1 shows the general synthetic route and the chemical structure of the NDT-based polymers. The synthesis of PNNT3BT is described in a previous report (shown as PNNTBT),⁴³ and the syntheses of NDT1, NDT2, and NDT4 are reported in a recent publication.⁴⁸ NDTs were distannylated by the lithiation at the α -position of fused thiophene rings with *n*-butyl lithium and sequential treatment with trimethyltin chloride to give 1–4. 1–4 and dibromo-dialkylbithiophene with $C_{16}H_{33}$ (C16) and $C_{20}H_{41}$ (C20) side chains were copolymerized via the conventional Stille coupling reaction to afford PNNT*m*BT-*l* ($m = 1-4, l = 16, 20$; e.g., PNNT1BT-16 stands for the polymer with NDT1 as the core and $C_{16}H_{33}$ as the side chains). All polymers were soluble in hot chlorobenzene, *o*-dichlorobenzene, and 1,2,4-trichlorobenzene, where the solubility was PNNT2BT > PNNT1BT > PNNT3BT > PNNT4BT from the highest, and the polymers with C20 side chains showed better solubility than those with C16 side chains. Molecular weights (M_n) of the polymers evaluated by high-temperature (140 °C) GPC calibrated with polystyrene standard were 21 000–52 000 g/mol (Table 1), which are assured to be sufficiently large; several different molecular weight batches were synthesized for some of the polymers, but the physical properties including the mobility were independent of the molecular weight as long as $M_n > 20\,000 \text{ g/mol}$ was achieved. All polymers were thermally stable up to 300 °C in DSC measurements (Figure S1). While polymers with C16 side chains did not show any

Table 1. Polymerization Results

polymer	side chain ^a	M_n (g/mol) ^b	M_w (g/mol) ^b	PDI	DP _n
PNNT1BT	C16	21 300	42 500	1.99	25.0
	C20	44 100	77 500	1.76	45.7
PNNT2BT	C16	27 900	49 000	1.76	32.8
	C20	21 700	42 400	1.95	22.5
PNNT3BT	C16	28 900	45 800	1.58	34.0
	C20	33 400	72 600	2.17	34.6
PNNT4BT	C16	29 500	46 500	1.58	34.7
	C20	52 100	104 900	2.01	54.0

^a C16 = hexadecyl ($C_{16}H_{33}$), C20 = icosyl ($C_{20}H_{41}$). ^b Evaluated from high-temperature GPC at 140 °C calibrated with polystyrene standard.

peaks in the thermograms, polymers with C20 side chains showed a broad peak at around 50 °C in both heating and cooling processes that can probably be assigned to the side chain melting.⁸⁴

Optical Properties. UV–vis absorption spectra of the polymers with C16 side chains (PNNT*m*BT-16; $m = 1-4$) in the chlorobenzene solution (10^{-5} – 10^{-6} mol/L) at room temperature (solution, blue lines) and at ca. 100 °C (hot solution, yellow lines), and in the spin-coated thin film from the chlorobenzene solution (as-spun, green lines) and the thin film after annealing at 150 °C for 30 min (annealed film, red lines), are shown in Figure 3a–d, respectively, and the absorption maxima (λ_{max}) are summarized in Table 2. The polymers with C20 side chains provided spectra similar to those with C16, and therefore we here focus on the polymers with C16 side chains. In the room temperature solution (blue lines), PNNT1BT-16, PNNT3BT-16, and PNNT4BT-16 gave well-defined spectra with two peaks and a shoulder at the shorter wavelength region, that is, 532 and 571 nm, 506 and 540 nm, and 492 and 529 nm, respectively, which are mostly identical to those in the as-spun thin film (green lines). This suggests that these three polymers have highly ordered backbone structures and strong π – π interactions (partial aggregation) in the solution.¹⁸ PNNT2BT-16, on the other hand, gave a single peak with λ_{max} of 487 nm in the solution, which slightly broadens toward the longer wavelength region, in the as-spun thin film, suggesting that PNNT2BT-16 has a less ordered backbone structure. When the solutions were heated (yellow lines), absorption peaks were significantly blue-shifted in PNNT1BT-16 ($\lambda_{\text{max}} = 495 \text{ nm}$) and PNNT3BT-16 ($\lambda_{\text{max}} = 454 \text{ nm}$) and slightly blue-shifted in PNNT2BT-16 ($\lambda_{\text{max}} = 476 \text{ nm}$), most likely reflecting the disaggregation at high temperature. Meanwhile, in PNNT4BT-16 the λ_{max} did not change, and instead the spectrum broadened toward shorter wavelength region, and the peak at 529 nm weakened. This suggests that PNNT4BT-16 tends to aggregate still in the high temperature solution, which is in good agreement with the fact that PNNT4BT-16 is the least soluble polymer among the four. Annealing the polymer thin films at 150 °C slightly red-shifted the λ_{max} only for PNNT3BT-16.

In the hot solution spectra, which in this case apparently reflect the electronic state of the isolated polymer chain, PNNT1BT-16 and PNNT2BT-16 provide λ_{max} at around 470–490 nm, which are located in the longer wavelength region than those for PNNT3BT-16 and PNNT4BT-16 that give λ_{max} at around 450 nm. Note that, for PNNT4BT-16, the shoulder that appears at around 450 nm should correspond to the isolated polymer chain, and the λ_{max} at 490 and 525 nm should be assigned to the absorption of ordered polymer chain. These results are apparently consistent with the results on DFT MO calculations at the B3LYP-6-31 g(d) level carried out using dithienonaphthodithiophenes (NDT*m*BT), the repeat units of the corresponding polymers, as model compounds (Figure 4). NDT1BT and NDT2BT with the linear-shaped core appeared to

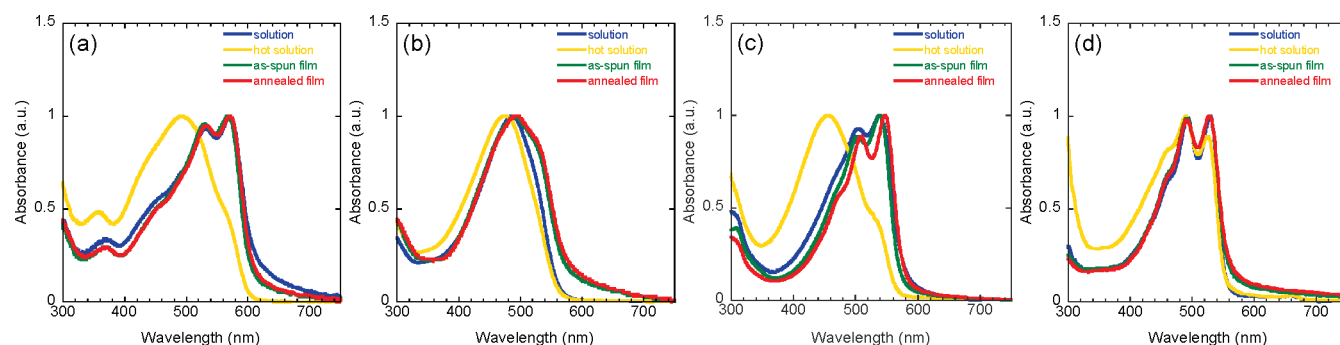


Figure 3. UV-vis absorption spectra of (a) PNDDT1BT-16, (b) PNDDT2BT-16, (c) PNDDT3BT-16, and (d) PNDDT4BT-16 in the chlorobenzene solution at room temperature (solution, blue lines), the chlorobenzene solution at ca. 100 °C (hot solution, yellow lines), the thin film spin-coated from the chlorobenzene solution (as-spun film, green lines), and the spin-coated thin film after annealing at 150 °C for 30 min (annealed film, red lines).

Table 2. Optical Properties of the Polymers with C16 Side Chains (PNDDT m BT-16)

polymer	λ_{\max} (nm)				IP (eV)
	solution	hot solution	as-spun film	annealed film	
PNDDT1BT-16	532, 571	495	530, 569	530, 570	5.1
PNDDT2BT-16	487	476	491	491	5.2
PNDDT3BT-16	506, 540	454	504, 539	509, 546	5.0
PNDDT4BT-16	492, 529	490, 525	491, 528	490, 528	5.1

have smaller bandgaps than did NDT3BT and NDT4BT with angular-shaped core, which can be understood by the nature that the linear-shaped and angular-shaped NDTs are isoelectronic with naphthalene and chrysene, respectively.⁴⁸

Photoelectron spectroscopy in air was carried out to evaluate the ionization potential (IP), that is, the HOMO level (E_{HOMO}), of the polymers in the thin film (Figure S2). As listed in Table 2, the IPs estimated from the onset of the spectra are 5.1, 5.2, 5.0, and 5.2 eV for PNDDT1BT–PNDDT4BT, respectively. Interestingly, the IP of PNDDT1BT was larger than that of PNDDT3BT, and similar to PNDDT4BT, which seemingly, in this case, disagrees with the calculation results for NDT m BTs shown in Figure 4. A plausible explanation can be described as follows by taking into account the calculated HOMOs of corresponding model compounds. In the linear NDTs (NDT1BT and NDT2BT), the HOMOs are apparently localized within the NDT cores, whereas in the angular NDTs (NDT3BT and NDT4BT) the HOMOs are delocalized over the whole molecular structures (including attached thiophene rings). Therefore, the elevation of the E_{HOMO} (ΔE_{HOMO}) from the parent NDTs to NDT m BTs is more significant in the angular NDT system as compared to the linear NDT system; for example, in the NDT1 system $\Delta E_{\text{HOMO}} (=E_{\text{HOMO}}(\text{NDTm}) - E_{\text{HOMO}}(\text{NDTmBT}))$ is ca. 0.10 (= $-5.09 - (-4.99)$) eV, whereas in the NDT3 system ΔE_{HOMO} is ca. 0.46 (= $-5.66 - (-5.20)$) eV. Assuming that this estimation can be adapted in the actual polymer system, the E_{HOMO} of the linear and angular NDT systems would get closer as the molecular chains extend to end up with the similar or possibly reversed E_{HOMO} , which well agrees with the results observed for the present polymer system.

OFET Characteristics. OFET characteristics of PNDDT m BTs were evaluated by top-contact, bottom-gate devices fabricated by using polymer thin films spin-coated from *o*-dichlorobenzene solutions onto hexamethyldisilazane (HMDS)- and 1H,1H,2H,

2H-perfluorodecyltriethoxysilane (FDTS)-modified Si/SiO₂ surfaces, respectively, which were subsequently annealed at 150 °C. Transfer and output curves of PNDDT m BT-16 devices on the HMDS-modified substrates and those of a PNDDT3BT-20 device on the FDTS-modified substrate are depicted in Figures 5 and 6, respectively. Relatively small hysteresis were observed in the transfer curves, and threshold voltages (V_T) for the HMDS-modified devices were around -10 V for all of the polymers. The positively shifted V_T for the FDTS-modified devices is attributed to the effects of electric dipoles of the SAM molecules and weak charge transfer between organic films and SAMs.⁴⁹ The output curves showed almost negligible nonlinear behavior in the low voltage regions that usually originates from contact resistance. Mobilities were calculated from the saturation regime and are listed in Table 3 together with on/off ratios. For polymers with C20 side chains, OFETs using the FDTS-modified substrates tended to give higher mobilities than those with the HMDS-modified substrates, which is most likely due to the lower surface energy as compared to the HMDS-modified devices, in turn promoting the higher molecular ordering of the polymers in the solid state.^{24,41,50} On the other hand, polymers with the C16 side chains were found to show lower mobilities in the FDTS-modified devices than in the HMDS-modified devices. This might be due to the difference of solubility and hence processability between these two polymers. Because the FDTS-modified Si/SiO₂ has a lower surface energy and thus is more sensitive to the process conditions as compared to the HMDS-modified Si/SiO₂ (FDTS-modified surface has a higher tendency to repel the polymer solutions), it is likely that the C20 polymers with higher solubility and viscosity can provide uniform films on the FDTS-modified surface, whereas the C16 polymers give nonuniform film, giving rise to the different trend in the mobility between the C16 and C20 polymers on each surface.

PNDDT3BT-20 on the FDTS-modified devices exhibited the highest mobility of $0.77 \text{ cm}^2 \text{ V}^{-1} \text{ s}^{-1}$ (average $0.38 \text{ cm}^2 \text{ V}^{-1} \text{ s}^{-1}$) with high on/off ratios of $\sim 10^7$. This value is among the highest observed so far for semiconducting polymers.^{20,23,24,51} The mobilities obtained for these polymers are PNDDT3BTs > PNDDT4BTs > PNDDT1BTs > PNDDT2BTs; for example, the average mobilities of the C20 polymers on the HMDS-modified devices are 0.18, 0.093, 0.027, and $0.0037 \text{ cm}^2 \text{ V}^{-1} \text{ s}^{-1}$, respectively. This trend is quite different from our initial expectation; we expected that PNDDT1BT would give the best performance, because NDT1 showed the highest mobility among the four NDT isomers in the small molecular systems.⁴⁸ To understand the difference of the mobility in these

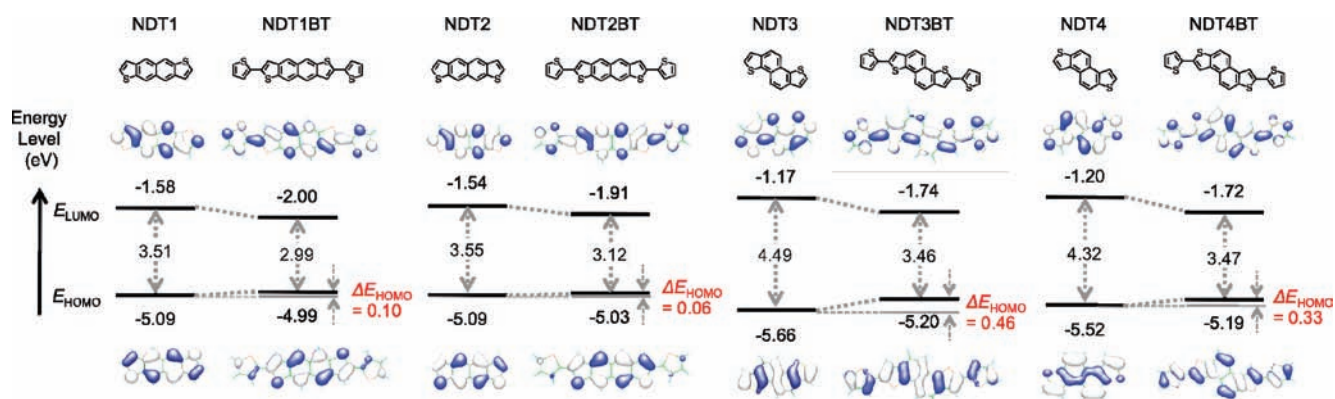


Figure 4. Calculated HOMOs and LUMOs of NDTs and the model compounds (NDT m BTs) of the polymers.

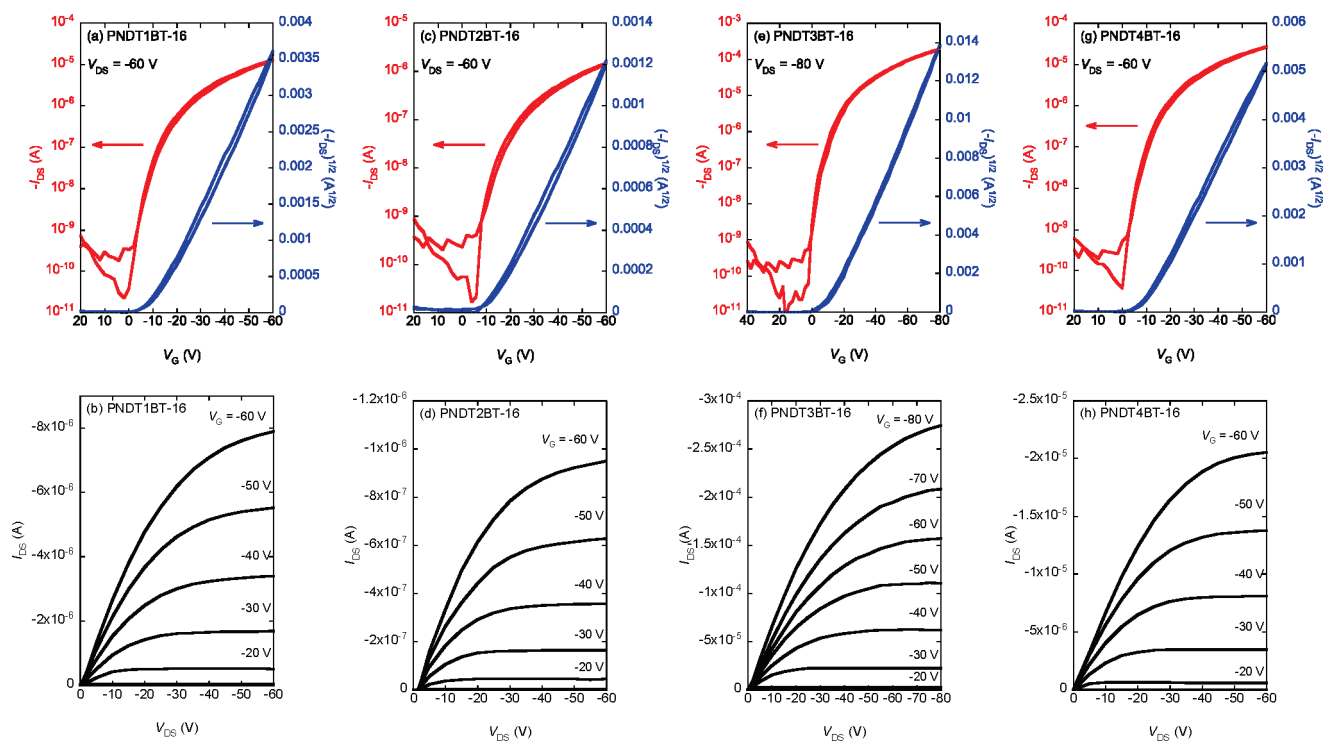


Figure 5. Transistor characteristics of PNDT m BT-16s: (a,c,e,g) transfer and (b) output curves of PNDT1BT-16, (c) transfer and (d) output curves of PNDT2BT-16, (e) transfer and (f) output curves of PNDT3BT-16, and (g) transfer and (h) output curves of PNDT4BT-16.

polymers and their unexpected trend, we carefully studied the ordering structures using grazing incidence X-ray diffraction (GIXRD) measurements, which will be discussed later in the following section.

In addition, to evaluate the environmental stability of the polymer devices, the devices were stored in air with relative humidity (RH) of ca. 50% for several months. Figure 7 depicts the changes in the transfer curves of the polymer devices for PNDT1BT-16 (a), PNDT2BT-16 (b), PNDT3BT-16 (c), PNDT4BT-16 (d), and PNDT3BT-20 (e). Reflecting the larger IP, PNDT1BT-16, PNDT2BT-16, and PNDT4BT-16 showed higher stability than PNDT3BT-16. It should be noted that as PNDT3BT-20 showed better stability as compared to PNDT3BT-16, longer alkyl chain can help to improve the environmental stability, possibly because the longer alkyl chains protect

the polymer backbone from ambient air and thereby humidity and oxygen, which would degrade device performances.³⁵

Ordering Structures and Their Correlations with Carrier Transport Properties. Ordering structures of the PNDT m BT-16 in the thin films were studied by grazing incidence X-ray diffraction (GIXRD) measurements. Out-of-plane (a) and in-plane (b) diffraction patterns of the polymer thin films annealed at 150 °C are shown in Figure 8. The out-of-plane patterns gave sharp peaks assignable to ($h00$), where (100) peaks appeared at around $2\theta = 4.2^\circ$, and d -spacings (d_1) of 20–22 Å, which correspond to the lamellar structure along with side chain interdigitation.^{18–20,43} Because these ($h00$) peaks were not seen in the in-plane patterns (although Figure 8b ranges only $2\theta = 15–30^\circ$, no peaks were seen when scanned for $2\theta = 0–15^\circ$), the polymers are dominantly edge-on oriented respective to the

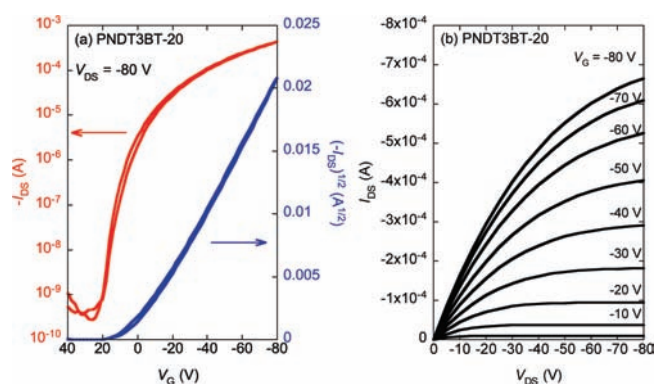


Figure 6. (a) Transfer and (b) output curves of an OFET device with PNNDT3BT-20 after annealing.

Table 3. Mobilities and On/Off Ratios of OFETs Based on PNNDT m BT- l^a

polymer	side chain	μ (cm ² V ⁻¹ s ⁻¹) ^b			I_{on}/I_{off}
		HMDS	FDTS		
PNNDT1BT	C16	0.029 (0.025)	0.024 (0.020)		$\sim 10^6$
	C20	0.037 (0.027)	0.055 (0.032)		$\sim 10^4$
PNNDT2BT	C16	0.0059 (0.0039)	0.0033 (0.0019)		$\sim 10^5$
	C20	0.0066 (0.0037)	0.026 (0.0016)		$\sim 10^3$
PNNDT3BT	C16	0.54 (0.20)	0.26 (0.12)		$\sim 10^7$
	C20	0.32 (0.18)	0.77 (0.38)		$\sim 10^7$
PNNDT4BT	C16	0.086 (0.043)	0.030 (0.022)		$\sim 10^7$
	C20	0.15 (0.093)	0.19 (0.14)		$\sim 10^7$

^a Bottom-gate top-contact devices with $L = 50 \mu\text{m}$, $W = 1500 \mu\text{m}$ were used, and the polymer films were annealed at 150°C for 30 min before deposition of Au source and drain electrodes. ^b Maximum mobilities and average mobilities in the parentheses from more than 10 devices.

substrate. It was found that, interestingly, each polymer gave quite distinct diffraction features in the out-of-plane direction (Figure 8a). PNNDT3BT-16 provides ($h00$) peaks up to the fourth order, the third order for PNNDT4BT-16, the second order for PNNDT1BT-16, and only the first order for PNNDT2BT-16, indicating that PNNDT3BT-16 forms the most highly ordered structure in the thin film and the rest of the polymers follow in this order.

It is also clear from the in-plane diffractions (Figure 8b) that PNNDT3BT-16 forms the most ordered structure. PNNDT3BT-16 exhibited a very strong (010) peak at $2\theta = 24.5^\circ$ corresponding to the π -stacking order between facing backbones with a distance (d_π) of 3.6 \AA , along with a small peak at $2\theta = 20.0^\circ$ most likely assignable to (004), the backbone repeat unit.^{22,52} PNNDT4BT-16 also showed a sharp (010) peak ($d_\pi = 3.6 \text{ \AA}$), but without a diffraction peak corresponding to the backbone repeat unit. It is noteworthy that this d_π of 3.6 \AA for these two polymers is smaller than those of so far reported high-performance semiconducting polymers that typically possess $3.7\text{--}3.8 \text{ \AA}$.^{18,20,25,29} These indicate that PNNDT3BT has a more ordered backbone structure than PNNDT4BT, although the π -stacking crystallinity seems to be comparable. On the other hand, in PNNDT1BT-16 a diffraction corresponding to (010) was barely seen at around $2\theta = 24.0^\circ$ ($d_\pi = \text{ca. } 3.7 \text{ \AA}$), indicative of very weak π -stacking crystallinity. In PNNDT2BT-16, although some unassignable diffraction peaks appeared at $2\theta = 16\text{--}22^\circ$, no peak was found at around $2\theta = 24\text{--}25^\circ$, indicating that

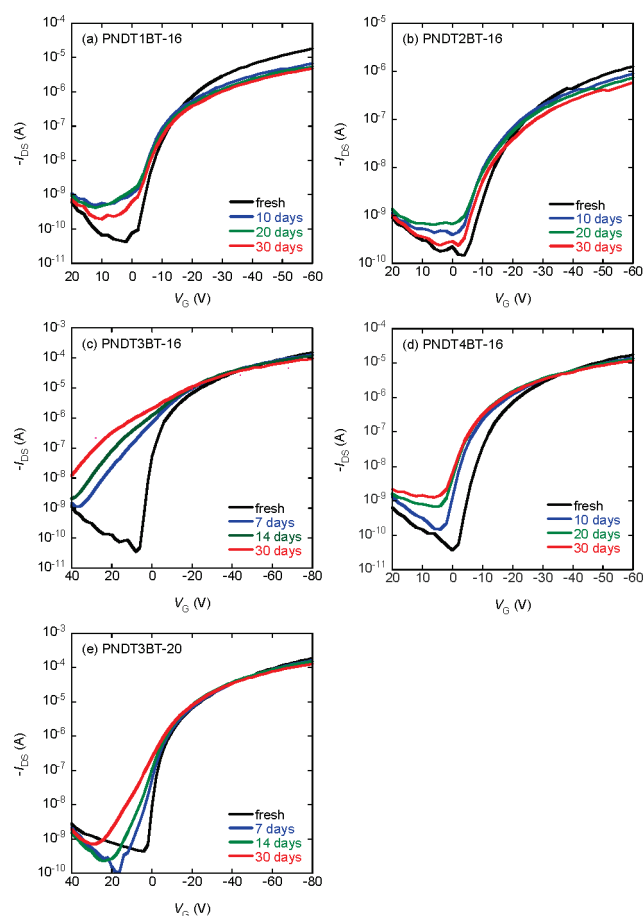


Figure 7. Changes in the transfer characteristic of polymer devices by time upon exposure to air (RH $\sim 50\%$): (a) PNNDT1BT-16, (b) PNNDT2BT-16, (c) PNNDT3BT-16, (d) PNNDT4BT-16, and (e) PNNDT3BT-20.

the π -stacking order is absent. The ordering structure is one of the most important parameters for the charge carrier transport, and it is mostly accepted that the higher mobility would be achieved as the ordering structure is enhanced. Hence, these results perfectly agree with the order of the mobility for these polymers as shown above.

To further understand the nature of the distinct ordering structure in these isomeric NDT-based polymers, we focused on the plausible polymer chain structures illustrated in Figure 9. It turns out that in the linear-NDT system, although both NDT1 and NDT2 give linear-shaped repeat units as shown in Figure 4, the molecular shapes of the corresponding polymer chains are not the case; PNNDT1BT and PNNDT2BT provide a zigzag and a square-wave shape, respectively. In the angular-NDT system, while PNNDT3BT gives a pseudostraight shape, PNNDT4BT gives a sine-wave shape with a short pitch. It is now quite understandable that having the relatively straight backbone, PNNDT3BT is likely to afford the most highly ordered structure among the four isomeric NDT systems. Although PNNDT4BT is unlikely to order efficiently considering its backbone shape, the spatially dense aromatic rings due to the short pitch of the curved backbone might help the π - π interaction and thus the molecular ordering. The zigzag or the square-wave shape of PNNDT1BT and PNNDT2BT, which are far from straight shape, would interfere with the ordering.

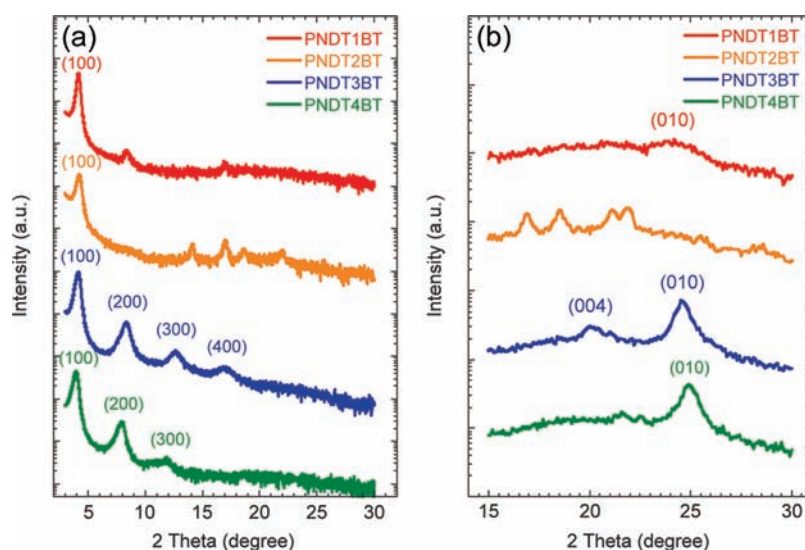


Figure 8. Out-of-plane (a) and in-plane (b) GIXRD patterns of PNDT m BT-16 in the annealed thin film. The lamellar d -spacings evaluated from (100) diffractions are 21.0 Å (PNDT1BT-16), 20.8 Å (PNDT2BT-16), 21.2 Å (PNDT3BT-16), and 22.3 Å (PNDT4BT-16), and the π -stacking distances evaluated from (010) diffractions are 3.7 Å (PNDT1BT-16) and 3.6 Å (PNDT3BT-16 and PNDT4BT-16). Note that the diffraction peak corresponding to the π -stacking for PNDT2BT-16 was absent, and thus the distance could not be determined.

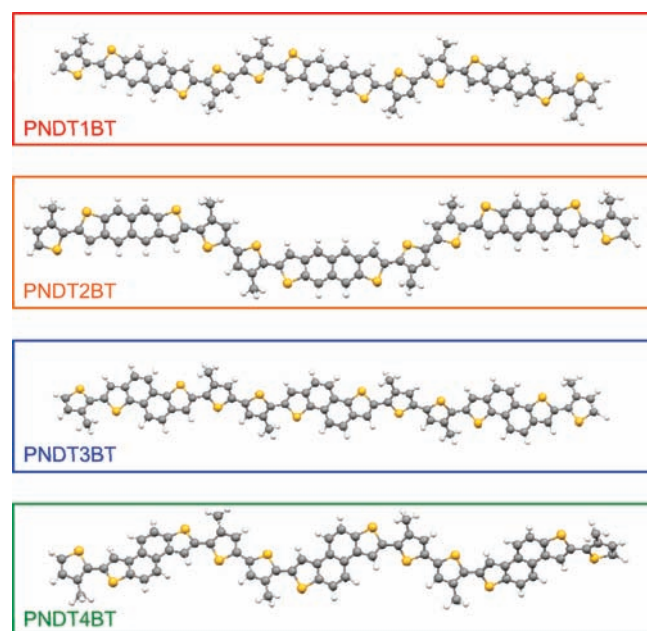


Figure 9. Optimized backbone structures of the polymers. The side chains were replaced with methyl groups to simplify the calculation.

Influence of Electronic Structures on Carrier Transport Properties. As described above, differences of the mobility in NDT-based polymers are mostly understood by correlating their ordering structures in the thin films. Meanwhile, we speculate that the extent of the HOMO delocalization also plays an important role in determining the charge carrier transport property. As indicated in an earlier section and in Figure 4, the HOMOs of PNDT1BT and PNDT2BT are relatively localized within the NDT core, which might then reduce the possibility of HOMO overlaps between face-to-face π -stacked polymer chains, giving rise to the limited charge carrier transport via the

π -stacking. On the other hand, the delocalized HOMOs in PNDT3BT and PNDT4BT would promote the efficient HOMO overlaps through the whole backbone, and thereby it would facilitate the efficient charge carrier transport. This speculation well agrees with the fact that PNDT3BT and PNDT4BT demonstrate 1 or 2 order higher mobilities than do PNDT1BT and PNDT2BT, respectively.

CONCLUSIONS

We have synthesized new semiconducting polymers by incorporating different isomeric NDTs. All polymers are sufficiently soluble in organic solvents and thus have good processability in solution-processed device fabrications. NDT3-based polymers exhibited the highest mobilities, $\sim 0.8 \text{ cm}^2 \text{ V}^{-1} \text{ s}^{-1}$, among the four NDT-based polymers, which are among the highest reported for semiconducting polymers to date. Furthermore, very interestingly, the charge carrier transport properties of these isomeric NDTs in the polymer system are found to give different trends from the small-molecule system. While NDT1 having a linear-shape and the anti sulfur position has shown the best mobility in the small-molecule system, angular-shaped NDT3 and NDT4 exhibited better mobilities than NDT1 in the polymer system. Grazing incidence X-ray diffraction studies revealed that the trend of the mobility in these polymers is completely consistent with the ordering structures; NDT3-based polymer gave the most highly ordered structure with the very close π -stacking distance of 3.6 Å, and NDT-4-based polymer gave a similar but less ordered structure, whereas the NDT1-based polymer had a very weak π -stacking order with a relatively wide distance of 3.7 Å, and no π -stacking order was observed for the NDT2-based polymer. These microstructures in the thin film can be well understood by considering their molecular shapes; although NDT1 has a linear shape and NDT3 has an angular shape, actually the NDT1- and NDT3-based polymers form a zigzag-shaped backbone and a pseudostraight backbone, respectively, the latter of which can effectively pack into the highly ordered structure. In addition, the delocalized HOMOs along the

backbone as seen for the NDT3- and NDT4-based polymers, in contrast to the relatively localized HOMOs in the NDT1- and NDT2-based polymers, would provide the efficient HOMO overlaps between the face-to-face π -stacked polymer chains and thus facilitate the charge carrier transport. Altogether, we conclude that the NDT3 is the most promising heteroarene core for the semiconducting polymers among the available NDTs. We also propose that the electronic structure as well as the molecular shape would be of particular importance to be taken into account when designing high-performance semiconducting polymers for organic electronics.

■ ASSOCIATED CONTENT

S Supporting Information. Complete list of authors for ref 21, synthesis, experimental procedures, DSC curves, photoelectron spectra, and AFM images of the polymers. This material is available free of charge via the Internet at <http://pubs.acs.org>.

■ AUTHOR INFORMATION

Corresponding Author

iosaka@hiroshima-u.ac.jp; ktakimi@hiroshima-u.ac.jp

■ ACKNOWLEDGMENT

This work is supported by the Strategic Promotion of Innovative Research and Development from the Japan Science and Technology Agency, Grants-in-Aid for Young Scientist B (no. 22750172), and Grants-in-Aid for Scientific Research B (no. 2035008800). I.O. is also grateful to the Sumitomo Foundation for financial support. We are grateful to Sumitomo Chemical Co., Ltd., for the measurement of photoelectron spectra and to Rigaku Corp. for the in-plane XRD measurement.

■ REFERENCES

- (1) Klauk, H. *Organic Electronics*; Wiley-VCH Verlag GmbH & Co. KGaA: Weinheim, Germany, 2006.
- (2) Bao, Z.; Locklin, J. *Organic Field-Effect Transistors*; CRC Press: Boca Raton, FL, 2007.
- (3) Crone, B.; Dodabalapur, A.; Lin, Y. Y.; Filas, R. W.; Bao, Z.; LaDuca, A.; Sarpeshkar, R.; Katz, H. E.; Li, W. *Nature* **2000**, *403*, 521–523.
- (4) Dimitrakopoulos, C. D.; Malenfant, P. R. L. *Adv. Mater.* **2002**, *14*, 99–117.
- (5) Garnier, F.; Hajlaoui, R.; Yassar, A.; Srivastava, P. *Science* **1994**, *265*, 1864–1866.
- (6) Bao, Z.; Feng, Y.; Dodabalapur, A.; Raju, V. R.; Lovinger, A. J. *Chem. Mater.* **1997**, *9*, 1299–1301.
- (7) Sirringhaus, H.; Kawase, T.; Friend, R. H.; Shimoda, T.; Inbasekaran, M.; Wu, W.; Woo, E. P. *Science* **2000**, *290*, 2123–2126.
- (8) Leclerc, M.; Morin, J.-F. *Design and Synthesis of Conjugated Polymers*; Wiley-VCH Verlag GmbH & Co. KGaA: Weinheim, Germany, 2010.
- (9) Skotheim, T. A.; Reynolds, J. R. *Handbook of Conducting Polymers*, 3rd ed.; CRC Press: Boca Raton, FL, 2007.
- (10) Bao, Z.; Dodabalapur, A.; Lovinger, A. J. *Appl. Phys. Lett.* **1996**, *69*, 4108–4110.
- (11) Sirringhaus, H. *Adv. Mater.* **2005**, *17*, 2411–2425.
- (12) Sirringhaus, H.; Brown, P. J.; Friend, R. H.; Nielsen, M. M.; Bechgaard, K.; Langeveld-Voss, B. M. W.; Spiering, A. J. H.; Janssen, R. A. J.; Meijer, E. W.; Herwig, P.; De Leeuw, D. M. *Nature* **1999**, *401*, 685–688.

- (13) McCullough, R. D.; Lowe, R. D. *J. Chem. Soc., Chem. Commun.* **1992**, 70–2.
- (14) Chen, T. A.; Rieke, R. D. *J. Am. Chem. Soc.* **1992**, *114*, 10087–8.
- (15) McCullough, R. D. *Adv. Mater.* **1998**, *10*, 93–116.
- (16) Osaka, I.; McCullough, R. D. *Acc. Chem. Res.* **2008**, *41*, 1202–1214.
- (17) Gallazzi, M. C.; Castellani, L.; Marin, R. A.; Zerbi, G. *J. Polym. Sci., Part A: Polym. Chem.* **1993**, *31*, 3339–3349.
- (18) Ong, B. S.; Wu, Y.; Liu, P.; Gardner, S. *J. Am. Chem. Soc.* **2004**, *126*, 3378–3379.
- (19) Kline, R. J.; DeLongchamp, D. M.; Fischer, D. A.; Lin, E. K.; Richter, L. J.; Chabynyc, M. L.; Toney, M. F.; Heeney, M.; McCulloch, I. *Macromolecules* **2007**, *40*, 7960–7965.
- (20) McCulloch, I.; Heeney, M.; Bailey, C.; Genevicius, K.; MacDonald, I.; Shkunov, M.; Sparrowe, D.; Tierney, S.; Wagner, R.; Zhang, W.; Chabynyc, M. L.; Kline, R. J.; McGehee, M. D.; Toney, M. F. *Nat. Mater.* **2006**, *5*, 328–333.
- (21) McCulloch, I.; et al. *Adv. Mater.* **2009**, *21*, 1091–1109.
- (22) Chabynyc, M. L.; Toney, M. F.; Kline, R. J.; McCulloch, I.; Heeney, M. *J. Am. Chem. Soc.* **2007**, *129*, 3226–3237.
- (23) Hamadani, B. H.; Gundlach, D. J.; McCulloch, I.; Heeney, M. *Appl. Phys. Lett.* **2007**, *91*, 24.
- (24) Umeda, T.; Kumaki, D.; Tokito, S. *J. Appl. Phys.* **2009**, *105*, 024516.
- (25) Pan, H.; Li, Y.; Wu, Y.; Liu, P.; Ong, B. S.; Zhu, S.; Xu, G. *J. Am. Chem. Soc.* **2007**, *129*, 4112–4113.
- (26) Ong, B. S.; Wu, Y.; Li, Y.; Liu, P.; Pan, H. *Chem.-Eur. J.* **2008**, *14*, 4766–4778.
- (27) Li, J.; Qin, F.; Li, C. M.; Bao, Q.; Chan-Park, M. B.; Zhang, W.; Qin, J.; Ong, B. S. *Chem. Mater.* **2008**, *20*, 2057–2059.
- (28) Rieger, R.; Beckmann, D.; Pisula, W.; Steffen, W.; Kastler, M.; Mullen, K. *Adv. Mater.* **2010**, *22*, 83–6.
- (29) Fong, H. H.; Pozdin, V. A.; Amassian, A.; Malliaras, G. G.; Smilgies, D.-M.; He, M.; Gasper, S.; Zhang, F.; Sorensen, M. *J. Am. Chem. Soc.* **2008**, *130*, 13202–13203.
- (30) He, M. Q.; Li, J. F.; Sorensen, M. L.; Zhang, F. X.; Hancock, R. R.; Fong, H. H.; Pozdin, V. A.; Smilgies, D. M.; Malliaras, G. G. *J. Am. Chem. Soc.* **2009**, *131*, 11930–11938.
- (31) Usta, H.; Lu, G.; Facchetti, A.; Marks, T. J. *J. Am. Chem. Soc.* **2006**, *128*, 9034–9035.
- (32) Liu, J.; Zhang, R.; Sauve, G.; Kowalewski, T.; McCullough, R. D. *J. Am. Chem. Soc.* **2008**, *130*, 13167–13176.
- (33) Rieger, R.; Beckmann, D.; Pisula, W.; Kastler, M.; Mullen, K. *Macromolecules* **2010**, *43*, 6264–6267.
- (34) Osaka, I.; Sauve, G.; Zhang, R.; Kowalewski, T.; McCullough, R. D. *Adv. Mater.* **2007**, *19*, 4160–4165.
- (35) Osaka, I.; Zhang, R.; Sauve, G.; Smilgies, D.-M.; Kowalewski, T.; McCullough, R. D. *J. Am. Chem. Soc.* **2009**, *131*, 2521–2529.
- (36) Osaka, I.; Zhang, R.; Liu, J.; Smilgies, D.-M.; Kowalewski, T.; McCullough, R. D. *Chem. Mater.* **2010**, *22*, 4191–4196.
- (37) Zhang, M.; Tsao Hoi, N.; Pisula, W.; Yang, C.; Mishra Ashok, K.; Mullen, K. *J. Am. Chem. Soc.* **2007**, *129*, 3472–3.
- (38) Burgi, L.; Turbiez, M.; Pfeiffer, R.; Bienewald, F.; Kirner, H.-J.; Winnewisser, C. *Adv. Mater.* **2008**, *20*, 2217–2224.
- (39) Liu, J.; Zhang, R.; Osaka, I.; Mishra, S.; Javier, A. E.; Smilgies, D.-M.; Kowalewski, T.; McCullough, R. D. *Adv. Funct. Mater.* **2009**, *19*, 3427–3434.
- (40) Guo, X. G.; Kim, F. S.; Jenekhe, S. A.; Watson, M. D. *J. Am. Chem. Soc.* **2009**, *131*, 7206–7207.
- (41) Osaka, I.; Takimiya, K.; McCullough, R. D. *Adv. Mater.* **2010**, *22*, 4993–4997.
- (42) Rieger, R.; Beckmann, D.; Mavrinskiy, A.; Kastler, M.; Mullen, K. *Chem. Mater.* **2010**, *22*, 5314–5318.
- (43) Osaka, I.; Abe, T.; Shinamura, S.; Miyazaki, E.; Takimiya, K. *J. Am. Chem. Soc.* **2010**, *132*, 5000–5001.
- (44) Shinamura, S.; Miyazaki, E.; Takimiya, K. *J. Org. Chem.* **2010**, *75*, 1228–1234.
- (45) Takimiya, K.; Ebata, H.; Sakamoto, K.; Izawa, T.; Otsubo, T.; Kunugi, Y. *J. Am. Chem. Soc.* **2006**, *128*, 12604–12605.

- (46) Ebata, H.; Izawa, T.; Miyazaki, E.; Takimiya, K.; Ikeda, M.; Kuwabara, H.; Yui, T. *J. Am. Chem. Soc.* **2007**, *129*, 15732–15733.
- (47) Izawa, T.; Miyazaki, E.; Takimiya, K. *Adv. Mater.* **2008**, *20*, 3388–3392.
- (48) Shinamura, S.; Osaka, I.; Miyazaki, E.; Nakao, A.; Yamagishi, M.; Takeya, J.; Takimiya, K. *J. Am. Chem. Soc.* **2011**, *133*, 5024–5035.
- (49) Kobayashi, S.; Nishikawa, T.; Takenobu, T.; Mori, S.; Shimoda, T.; Mitani, T.; Shimotani, H.; Yoshimoto, N.; Ogawa, S.; Iwasa, Y. *Nat. Mater.* **2004**, *3*, 317–322.
- (50) Nakayama, K.; Uno, M.; Nishikawa, T.; Nakazawa, Y.; Takeya, J. *Org. Electron.* **2010**, *11*, 1620–1623.
- (51) Li, Y.; Singh, S. P.; Sonar, P. *Adv. Mater.* **2010**, *22*, 4862–4866.
- (52) DeLongchamp, D. M.; Kline, R. J.; Jung, Y.; Germack, D. S.; Lin, E. K.; Moad, A. J.; Richter, L. J.; Toney, M. F.; Heeney, M.; McCulloch, I. *ACS Nano* **2009**, *3*, 780–787.